AIP | Journal of Applied Physics

Magnetic pinning effects of epitaxial LaxSr1−xMnO3 nanostructured thin films on YBa2Cu3O7−δ layers

T. Petrisor, M. S. Gabor, C. Tiusan, V. Galluzzi, G. Celentano et al.

Citation: J. Appl. Phys. **112**, 053919 (2012); doi: 10.1063/1.4748049
View online: http://dx.doi.org/10.1063/1.4748049
View Table of Contents: http://jap.aip.org/resource/1/JAPIAU/v112/i5
Published by the American Institute of Physics.

Magnetic pinning effects of epitaxial $La_xSr_{1-x}MnO_3$ nanostructured thin films on $YBa_2Cu_3O_{7-\delta}$ layers

T. Petrisor, Jr.,[1,2] M. S. Gabor,[1] C. Tiusan,[1,2] V. Galluzzi,[3] G. Celentano,[3] S. Popa,[4] A. Boulle,[5] and T. Petrisor[1]
[1]*Centre for Superconductivity, Spintronics and Surface Science (C4S), Technical University of Cluj-Napoca, Str. Memorandumului nr. 28, 400114 Cluj-Napoca, Romania*
[2]*Institut Jean Lamour, UMR 7198 CNRS-Nancy Université, Vandœuvre-lès-Nancy, France*
[3]*Associazione EURATOM-ENEA sulla Fusione, Frascati Research Centre, Via E Fermi, 45, 00044 Frascati, Rome, Italy*
[4]*National Institute of Materials Physics, Bucharest, Magurele 077125, Romania*
[5]*Science des Procédés Céramiques et de Traitements de Surface (SPCTS), CNRS UMR 6638, Centre Européen de la Céramique, 12 rue Atlantis, 87068 Limoges, France*

(Received 11 April 2012; accepted 20 July 2012; published online 11 September 2012)

The present paper presents the effects of a nanostructured, ferromagnetic $La_{1-x}Sr_xMnO_3$(LSMO) thin film on the pinning characteristics of an epitaxial $YBa_2Cu_3O_7$(YBCO) thin film deposited on top. Ordered arrays of LSMO grains were obtained upon growing the film on a terraced (001) $SrTiO_3$ substrate. The analyses of magnetic measurements revealed the presence of a complex vortex pinning mechanism within the YBCO film. With respect to a reference single YBCO layer, an additional pinning potential was observed. Its temperature evolution suggests that a magnetic pinning mechanism is responsible for improved pinning characteristics in the high temperature and field region. Based on the morphology of the underlying LSMO buffer, a strong pinning force is expected to arise due to the anti-dot formations, where a high magnetization gradient exists. [http://dx.doi.org/10.1063/1.4748049]

I. INTRODUCTION

Large scale applications of superconductivity require type II superconducting materials which are able to transport high electrical currents in high magnetic field without losses. The vortex movement is the main mechanism limiting the critical current density, J_c, in the mixed state. The only way to avoid the vortex movement is to pin the vortices within the Abrikosov lattice. Therefore, pinning is crucial for producing superconducting materials with high critical current densities for power applications. The problem of pinning is especially important for high temperature superconductors (HTS) where, at temperatures close to T_c, depinning takes place by a thermal activation process, which increases exponentially with temperature. The conventional way to enhance pinning, both in low and high temperature superconductors (SCs), is to fabricate samples with nanometric normal defects. Because of the temperature dependence of the London penetration length, λ_L, condensation energy pinning, or core pinning, is mainly important at low temperatures. Moreover, in the case of HTS, the condensation energy pinning is not high enough to avoid depinning by thermal fluctuations, because of the small volume of the vortex core and the layered nature of HTS.[1] To increase the working temperature of HTS based applications, close to the critical temperature, T_c, the study of a new pinning mechanism, effective in the high temperature range, is necessary. Recently, it has been shown that magnetic pinning could represent a feasible solution for the problem of pinning in HTS materials. Bulaevskii *et al.*[2] have suggested that in a superconductor-ferromagnet (SC-FM) multilayer, the stripe domain structure within the FM layers modulates the magnetic field through the SC layers, and by means of a Zeeman interaction with the vortices, creates a periodic, temperature independent ($T \ll T_{Curie}$), magnetic pinning potential $U_{mp} \sim \Phi_0 M(x) d_s$, where $M(x)$ is the magnetization of the ferromagnetic film and d_s the thickness of the superconducting layer. The magnetic single vortex pinning energy was estimated to be two orders of magnitude larger than the pining energy for columnar defects.[2] The high value of U_{mp} and its weak temperature dependence is very important to overcome the thermal activation flux flow in HTS at temperatures close to T_c. Although not as studied as their low critical temperature (LTS) counterparts,[3,4] magnetic pinning has been demonstrated on HTS materials. For $YBa_2Cu_3O_7$ (YBCO) thin films, in particular, magnetic pinning has been demonstrated using ferromagnetic nanoparticle inclusions,[5] for which a double pinning mechanism, both normal core and magnetic, was observed. Also, magnetic pinning effects were generated by continuous ferromagnetic doped lanthanum manganite films. This class of materials is especially studied in relationship to YBCO thin films, as the two materials have an excellent structural compatibility, which allows for the epitaxial growth of heterostructures. Albrecht *et al.*[6] prepared $La_{2/3}Ca_{1/3}MnO_3$ /$SrTiO_3$ (STO)/$YBa_2Cu_3O_7$ heterostructures in which the doped lanthanum manganite thin film was subjected to a substrate induced compressive and tensile strains. In both cases, a magnetic pinning mechanism was observed. Chen *et al.*[7,8] used the ferromagnetic/anti-ferromagnetic phase separation, that occurs within $La_{0.67}Sr_{0.33}MnO_3$(LSMO) layers under certain strain conditions, to produce magnetic inhomogeneity that leads to a magnetic pinning force exerted on the flux lines of YBCO layers. Recently, Jha *et al.*[9] observed enhanced pinning characteristics of YBCO films deposited on LSMO nano-particle

decorated substrates. The pinning was ascribed to a double pinning mechanism, both normal core pinning, generated by the columnar defects presumably created within the SC film by the particles, as well as a magnetic pinning, present due to the ferromagnetic nature of the islands. Alternatively, cuprate/magnanite based heterostructures have been shown to exhibit an inverse superconducting spin switch behavior,[10,11] the origin of which has been recently proven to stem from the magnetic exchange field present at the $La_{0.7}Ca_{0.3}MnO_3/YBa_2Cu_3O_{7-\delta}$ interface.[12]

In the present paper, we investigate the pinning characteristics of an YBCO film deposited on a LSMO buffer layer. The particularity of the LSMO film resides in its surface morphology consisting of ordered arrays of LSMO grains aligned along the edges of the (001) $SrTiO_3$ substrate terraces. The superconducting properties are compared to those of a single YBCO film. A double pinning mechanism is observed in the bi-layered structure, which is ascribed to the normal core pinning and to a magnetic contribution to the overall pinning force. The magnetic pinning force is a consequence of the magnetization gradient present at the hole sites within the LSMO film.

II. EXPERIMENTAL

Single crystal (001) STO substrates were used for the deposition of the YBCO reference film and of the YBCO/LSMO bi-layer. In the case of the bi-layer, prior to the deposition of the LSMO buffer, the STO substrate underwent both a chemical and a thermal treatment. The two procedures were performed in order to ensure a uniform termination layer of the STO substrate and also to open the atomic level terraces on the substrate surface. The chemical treatment consisted of immersing the substrate in a NH_4OH buffered hydrofluoric acid (HF) solution for 5 s and neutralization in de-ionized water. Afterwards, the substrate was annealed at 1200 °C for 1 h in 15 l/h of flowing O_2. The LSMO thin film was deposited on the as treated substrate by means of dc magnetron sputtering. The deposition took place in a mixture of $Ar : O_2$ having a 3:1 ratio at a total pressure of 40 mTorr, from a stoichiometric, 2 in., $La_{0.66}Sr_{0.33}MnO_3$ target. During deposition, the substrate temperature was maintained at 800 °C. The YBCO films were deposited by means of pulsed laser deposition (PLD) using a XeCl laser at a repetition rate of 10 Hz and a laser energy of 120 mJ. The deposition was carried out at 850 °C in 290 mTorr of O_2. Cooling was performed in 3/4 atm of O_2 with a 15 min dwell at 450 °C, in order to stabilize the YBCO superconducting orthorhombic phase. Under these deposition conditions, both YBCO films have a thickness of 70 nm. The morphological properties of the treated substrate and that of the LSMO and YBCO films were investigated by means of AFM analysis using a Veeco Dimension 3100 microscope. Structural, x-ray characterization of the films was performed by a Bruker AXS D8 Discover diffractometer in a high resolution configuration. The magnetic measurements on the samples were done using a variable temperature VSM (Cryogenic Ltd.).

III. RESULTS AND DISCUSSION

A. Morphologic characterization

The AFM image of the as treated STO substrate surface, Figure 1 (upper panel), consists of terraces having a mean width of 182 nm and an average height of 0.4 nm. The lattice parameter of $SrTiO_3$ is of 3.905 Å, and hence the substrate step height indicates that one terrace corresponds to one lattice parameter. The deposition of a 35 nm thick LSMO thin film on the terraced substrates results in the formation of ordered arrays of LSMO grains along the STO steps, Figure 1 (lower panel). The regular nature of the film grains is due to the fact that substrate step corners represent energetically favorable nucleation sites for film growth.[13] As being the case, the terrace width will act so as to limit grain growth. Profile analysis of the AFM image reveals that the average extent of the LSMO grains in a direction perpendicular to the terrace border is of 133.8 ± 25.5 nm, in good agreement with the terrace width. Grain growth along the step edges is limited by the growth of the neighboring grains, so that the average grain width along the terraces is of 91.7 ± 13.1 nm. As far as the grain height is concerned, an asymmetry also exists along the two studied directions. Along the substrate terraces, due to coalescence, the island height is of only 1.1 ± 0.4 nm, while across the terraces, grain height is of 3.5 ± 0.4 nm. The areal density of the LSMO grains was found to be 92 grains/μm^2. Grain coalescence and the stepped nature of the substrate gave rise to the formation of "holes" in the LSMO film, located at the terrace border between several LSMO grains. If we consider that the film is elsewhere continuous, these holes may be

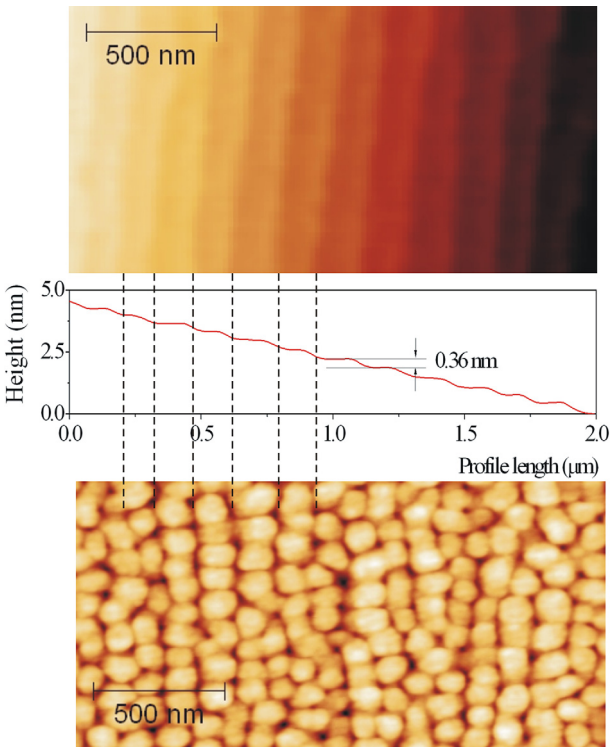

FIG. 1. 2 $\mu m \times 1$ μm AFM image of the terraced (001) STO substrate (upper panel); typical profile of the substrate (middle panel); 2 $\mu m \times 1$ μm AFM image of the LSMO buffer layer, LSMO grain width corresponds to the STO terrace width, as shown by the dotted lines (lower panel).

regarded as ordered arrays of "anti-dots" that lay alongside substrate steps. The average diameter of these features is of 30 ± 4 nm, while their areal density is of 80 holes/μm^2. Their reduced density with respect to that of the grains is to be expected, since the holes form at the intersection of several grains. As far as their depth is concerned, it coincides with the intra-step LSMO island height, 3.5 ± 0.4 nm. As it will be shown later, the presence of these features will play a crucial role in the determination of the flux pinning characteristics of the top YBCO film. The AFM images of the YBCO films are not shown here. The reference film, deposited directly onto a STO substrate, shows a relatively smooth surface having a low number of particulates present on the surface, inherent to the PLD deposition method.[14] In the case of the buffered YBCO film, the situation is different, as a high density of particulates may be observed, having a density as high as 575 particles/μm^2 and a mean lateral size of 91 nm. This finding has been previously reported by Aytug *et al.*[15] on LSMO buffered NiW tapes upon which YBCO was grown. Transmission electron microscopy (TEM) analysis revealed that these particulates are localized at the film surface and therefore can be neglected in the investigation of the vortex pinning characteristics.

B. Structural characterization

In order to quantify the influence of the LSMO template on the structural properties of the YBCO film, high resolution x-ray diffraction analysis was employed. $2\theta/\omega$-scans performed on both samples reveal an epitaxial growth of both YBCO films on the STO (001) substrate, as well as on the LSMO film, Figure 2. It is to be noted that LSMO was grown epitaxially on the STO substrate, as revealed by the $2\theta/\omega$ diffractogram recorded prior to the YBCO deposition. The out-of-plane epitaxial relationships describing the two samples are STO(001) || YBCO(001), for the reference YBCO film and STO(001) || LSMO(001) || YBCO(001), for the LSMO/YBCO bi-layer.

In order to test the epitaxial quality of the YBCO films, we have performed ω-scans around the (00 l) reflections. The results for the (002) reflections are presented in Figure 3. As it can be observed for the YBCO film grown on the LSMO buffer, the rocking curve is comprised a narrow component having a higher intensity and a lower intensity broad contribution. The presence of the diffuse part in the ω-scan originates from distorted regions that exist within the films around structural defects, such as dislocations, grain boundaries, or different kinds of inhomogeneities. On the other hand, the narrow component stems from the long range order that appears in high quality crystalline structures. Performing numerical simulations on the measured ω-scans, quantitative information may be derived concerning the spatial and statistical properties of the strain field around the distorted regions and the in plane structural coherence length ("crystallite" size).[16] In the present case, a good agreement between the calculated and the observed curves could be obtained assuming a Gaussian distribution of strain and crystallites having a parallelepiped shape. The strain field is characterized by an in-plane correlation length ξ, below which the lattice displacements are correlated, which in the case of a symmetrical reflection, correspond to the root-mean-squared (rms) rotations, i.e., the mosaicity. This mosaicity gives rise to the diffuse peak. Above the correlation length ξ, the displacements are uncorrelated so that the mosaicity drops down to zero, which gives rise to the coherent peak. The correlation length ξ, hence, corresponds to the spatial extension of the strain field which can be often be regarded as a mean distance between defects.[17] The simulations yielded a defect correlation length for the single YBCO film, $\xi_{YBCO} = 150$ nm and a mosaicity of $0.057°$. These values indicate a low defect density and an excellent structural quality. On the other hand, in the case of the YBCO/LSMO film, the correlation length, $\xi_{YBCO/LSMO} = 70$ nm and the mosaicity was calculated to be $0.22°$. The low value of $\xi_{YBCO/LSMO}$ indicates the presence of a higher number of defects. These defects give rise to higher strain values around them as evidenced by the high mosaicity. As it will be seen, the numerical interpretation of the ω-scans of the YBCO films prove to be valuable

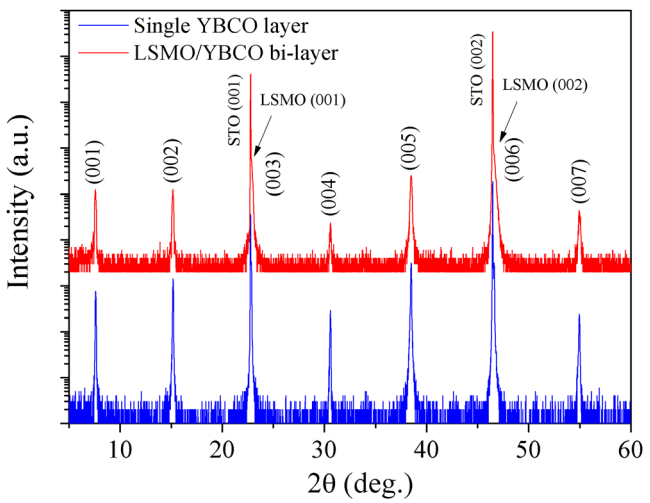

FIG. 2. $2\theta/\omega$ scans of the single YBCO film deposited on the STO substrate and of the YBCO/LSMO bi-layer. (00l) peaks correspond to the epitaxial YBCO films.

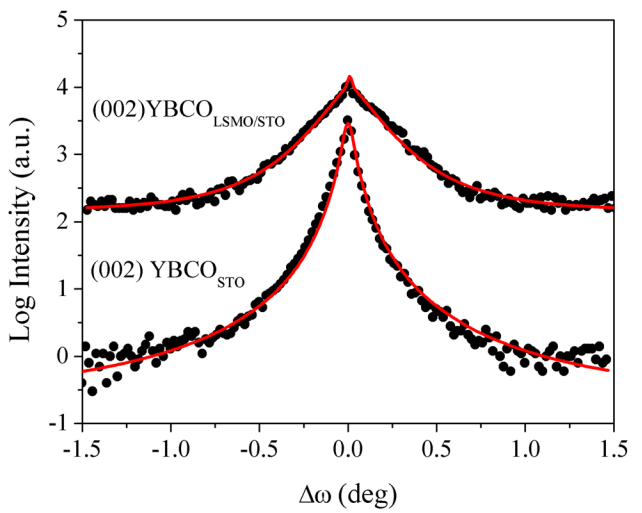

FIG. 3. ω-scans around the (002) reflections of the two YBCO films (circles) and the corresponding simulations (lines).

for the interpretation of the superconducting properties of the YBCO films.

C. Superconducting properties

The critical temperature of the two films was determined from the intersection of the field cooled (FC) and zero field cooled (ZFC) magnetization measurements. The T_c for the single YBCO layer was found to be 89.7 K, while for the buffered YBCO sample it was of 88.8 K.

Bean's critical state model was used to determine the critical current density J_c values, from $M(B)$ loops, according to the formula[18]

$$J_c = 20\frac{\Delta M}{w\left(1-\frac{w}{3l}\right)}, \quad (1)$$

where $\Delta M = M_+ - M_-$ represents the irreversible part of the magnetization, while w and l represent the width and length of the sample. The $M(B)$ measurements, Figure 4, were performed having the applied magnetic field oriented in a direction parallel to the c-axis of the YBCO films. Each branch of the $M(B)$ curves was fitted using a linear combination of exponential functions. The as-obtained fits were used in the determination of the critical current densities, $J_c(B)$, shown in Figure 5, for 10, 40, and 70 K, respectively. By comparing the $J_c(B)$ curves for the YBCO film grown directly on STO and those for the YBCO/LSMO bi-layer, two features may mainly be noted. First, at $B \approx 0$, the reference YBCO film has a higher J_c with respect to the YBCO film grown on the LSMO buffered STO substrate. A diminishing critical current density of YBCO layers deposited on top of LSMO films has been previously reported by Aytug *et al.*[15] and was ascribed to a Sr contamination of the superconducting film from the LSMO buffer. The second feature regards the magnetic field dependence of the critical currents. A closer examination of the $J_c(B)$ dependencies reveals that at low temperatures, 10 K, both samples show a similar magnetic field behavior. At the intermediate temperature of 40 K, a difference in the two $J_c(B)$ curves becomes apparent above 4 T. It may be observed that the critical current density corresponding to the YBCO layer starts to decrease more abruptly, while for the J_c of the YBCO film of the bi-layer, no change of the decrease rate could be observed. As the temperature is further increased, the difference between the two is directly observed, as above 3.5 T, the J_c of the YBCO within the bi-layer is higher than that of the single YBCO film. The lower slope of the J_c vs. B curve in the high magnetic field region ($B > 3.5$ T) is an indication of a stronger vortex pinning in the YBCO/LSMO film. This can be due to a higher core pinning density centers or to the existence of a second magnetic pinning mechanism.

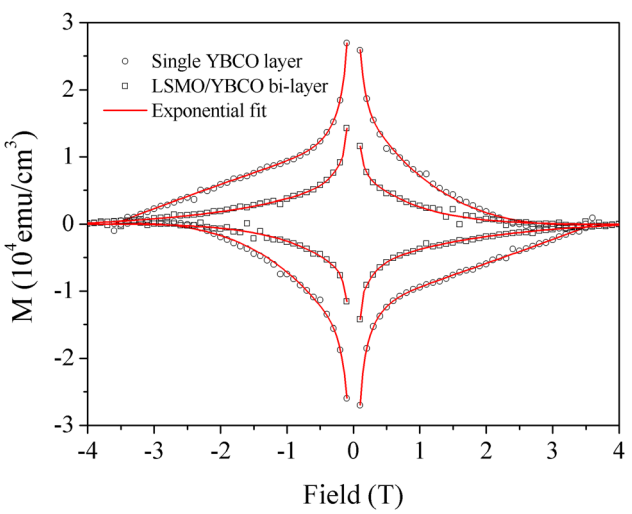

FIG. 4. Magnetization curves of the single YBCO film (open circles), the LSMO/YBCO bi-layer (open squares) measured at 70 K, and their corresponding fits (solid lines).

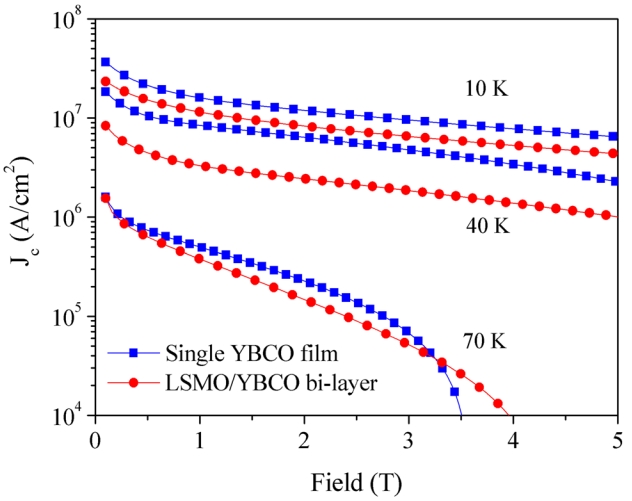

FIG. 5. Magnetic field dependence of the critical current density, J_c, as deduced from Eq. (1), at 10, 40, and 70 K.

The irreversibility field, H_{irr} is another important parameter in the evaluation of the strength of a pinning potential, as stronger pinning potentials shift the irreversibility line to higher field and temperature values. The irreversibility fields, Figure 6, were determined by linear extrapolation of the $J_c^{1/2}H^{1/4}(H)$ curve to the horizontal H axis, the Kramer plot technique (see, for example, Ref. 19). Good agreement was found between the as-determined H_{irr} values and those

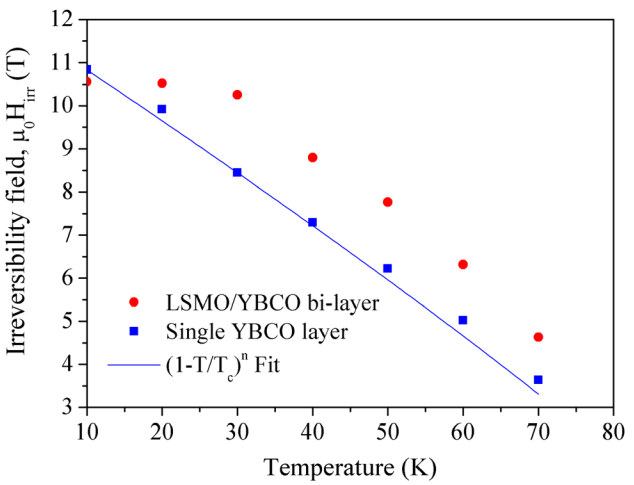

FIG. 6. Temperature dependence of the irreversibility field, $\mu_0 H_{irr}$, of the two YBCO samples.

determined directly from the $M(B)$ curves, in the high temperature range, where the hysteresis loops are closed. For example, a $\mu_0 H_{irr}$ value of 3.63 T was found for the single YBCO film at 70 K using the Kramer plot technique, while a direct determination yielded a value of 3.61 T. It can be observed that the irreversibility field of the YBCO film of the bi-layer is higher than that of the single YBCO layer. This confirms once again that above 10 K, vortex pinning in the YBCO/LSMO bi-layer is more effective. Another point in supporting the above hypotheses is the actual $H_{irr}(T)$ dependence. If for the single YBCO, it follows a $(1 - T/T_c)^n$ law, as shown in Figure 6, characteristic for YBCO thin films, the dependence of the YBCO film within the bi-layer does not follow a single law, which confirms the more complex pinning mechanism.

In type II superconductors, the existence of a single pinning mechanism results in a temperature scaling behavior of the pinning force density, $F_p = J_c B$, with the normalized magnetic field, $h = H/H_{irr}$. Figure 7 shows the $f(h)$ curves at different temperatures for the two samples, where $f = F_p/F_{p,max}$ is the normalized pinning force. The curves corresponding to the single YBCO film exhibit a scaling behavior.

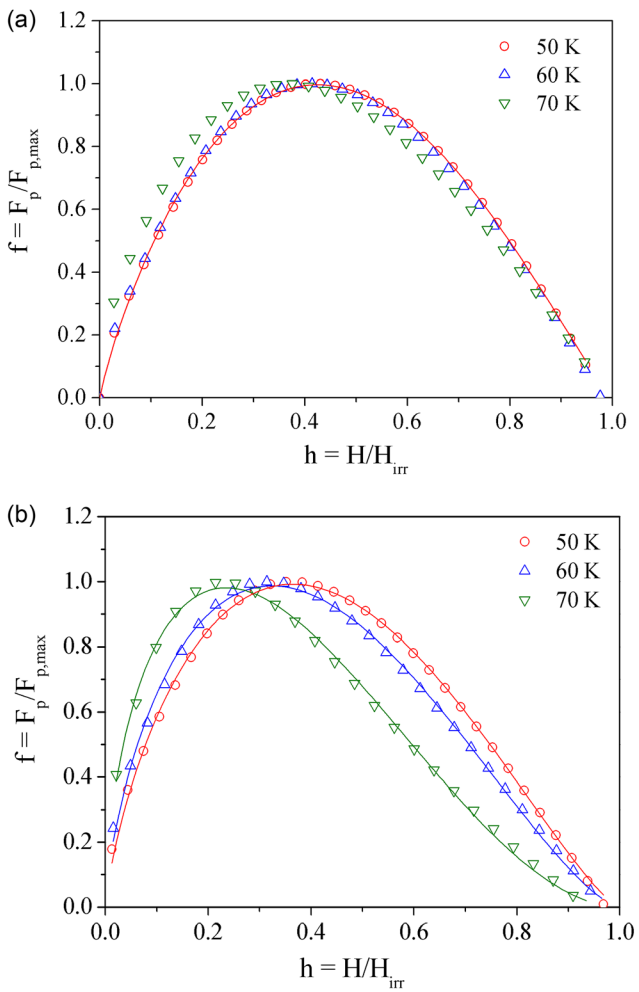

FIG. 7. $f(h)$ dependencies at different temperatures for (a) the single YBCO film and (b) for the YBCO layer deposited on the LSMO buffer (open symbols). Scaling law fit (solid lines), Eq. (2), of $f(h)$ for (a) the single YBCO film at 50 K and (b) for the buffered YBCO film for all the studied temperatures.

The presence of scaling is an indication of the existence of a single pinning mechanism within this film. The solid curve in Figure 7(a) shows a fit of the $f(h)$ dependence at 50 K, where the pinning force was expressed as (see, for example, Ref. 20)

$$F_p = A H_{irr}^m h^n (1-h)^p. \tag{2}$$

On the contrary, for the YBCO film grown on LSMO, the $f(h)$ curves, Figure 7(b), show a strong evolution with temperature, as the maximum pinning force value shifts towards lower h values as the temperature increases. This clearly indicates that, in this case, a second pinning mechanism is present. The presence of an additional pinning mechanism is also evident from the evolution with temperature of the scaling law parameter, p. All the $f(h)$ curves of the YBCO/LSMO sample could be fitted well with Eq. (2), however, p exhibited temperature variation. Figure 8 presents the temperature evolution of the scaling law parameter p of the two samples. For the single YBCO layer, in the studied temperature range, p has a value of 1.12 ± 0.1 that does not show significant temperature dependence, as was to be expected as a consequence of the observed scaling behavior. The variation of the p corresponding to the YBCO film within the bi-layer suggests that in the low temperature range, the vortex pinning mechanisms are similar for the two superconducting films, while at temperatures closer to T_c, a second pinning mechanism has a more pronounced influence on flux line lattice dynamics.

The temperature variation of the critical current density, $J_c(T)$ at constant fields, Figure 9, confirms the presence of second, stronger pinning potential at high temperatures in the YBCO/LSMO sample. In the low temperature range, up to 50 K, both current densities exhibit an exponential decay with temperature, according to a $J_c \propto \exp(-T/T_0)$ law, where T_0 is the characteristic temperature.[21] In the 50–70 K interval, the single YBCO film shows a more pronounced decrease with respect to the YBCO film grown on LSMO. As a consequence, the critical current density above 65 K is higher for the latter. The stronger pinning characteristic exhibited at high

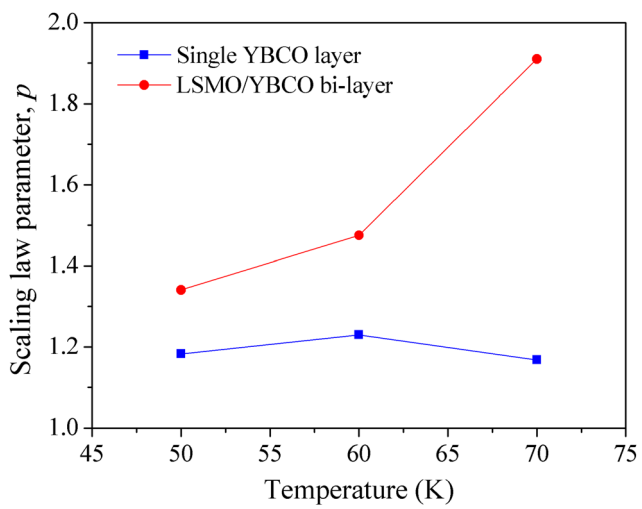

FIG. 8. Scaling law, Eq. (2), parameter p evolution as a function of temperature for the two YBCO films.

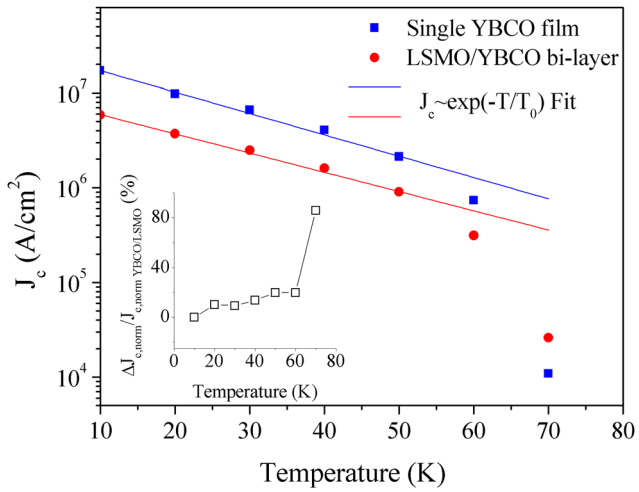

FIG. 9. $J_c(T)$ variation in an applied external field of 3.5 T for the two YBCO films; (inset) $\Delta J_{c,norm}/J_{c,normYBCO/LSMO}$, see Eq. (3), calculated at different temperatures for an applied field of 3.5 T.

temperatures for the YBCO/LSMO sample are also clearly visible in the inset of Figure 9, where the relative variation of the normalized critical current densities for the two films was plotted against temperature. The variation of the normalized critical current densities at different temperatures was calculated as

$$\Delta J_{c,norm} = \frac{J_{c,YBCO/LSMO}}{J_{c,YBCO/LSMO,max}} - \frac{J_{c,YBCO}}{J_{c,YBCO,max}}. \quad (3)$$

An increase in 86% in the relative variation of the normalized J_c was calculated for the YBCO/LSMO structure, suggesting that the second pinning mechanism responsible for the vortex lattice dynamics at high temperatures in this case becomes highly effective in the temperature range close to the critical temperature, T_c.

All the above analyses suggest that a second pinning mechanism, having a specific distinct temperature and field behavior is present in the YBCO/LSMO sample. This second pinning contribution is effective at high temperatures in high applied magnetic fields, as demonstrated by the $J_c(B)$ dependencies. Normal core pinning centers induced in the YBCO film by the surface irregularities of the LSMO layer may be excluded, as their density, 80 holes/μm^2, is too low to produce any significant changes in the pinning characteristics of the top YBCO film.[22] Numerical simulations of the ω-scans measured on both YBCO films indicated the presence of a higher density of defects within the YBCO/LSMO film, as the measured defect correlation length is almost two times lower than for the single film. However, the high mosaicity around these defects prevents them to act as effective normal core pinning centers and most likely they represent weak links between the superconducting regions within the film. In view of the above arguments, a lower critical current density in the case of the buffered YBCO sample may be explained by a reduction of the overall superconducting volume through the presence of weak links. The close values of H_{irr} of the two samples at 10 K, where core pinning is dominant, suggest that both samples posses an equal number of core pinning centers. Therefore, due to the ferromagnetic nature of LSMO, we propose magnetic pinning to be responsible for the additional observed contribution.

From a magnetic point of view, in this thickness range, strained LSMO films grown on STO (001) substrates exhibit an in-plane bi-axial anisotropy, together with an uniaxial in-plane contribution due to the terraced nature of the substrates.[23] The corresponding magnetic domain size is of about 1 μm.[24] Detailed structural investigation[25] revealed that LSMO thin films deposited in the present conditions grow fully strained on STO (001) substrates. Thus, the magnetic properties mentioned above are expected for the LSMO buffer layer. A magnetic pinning force arises whenever magnetic inhomogeneities are present within the magnetic structure found in the proximity of the superconducting layer. A low pinning force density is expected to exist due to the magnetization variation within the domain walls, due to the large domain size. On the other hand, this contribution vanishes as the film reaches out-of-plane saturation, $\mu_0 H_s \approx 1.5$ T,[26] and therefore cannot explain the pinning contribution at high fields, seen above 3.5 T in the $J_c(B)$ measurements. However, in the present case, due to the periodic modulation of the LSMO thickness, at saturation, a magnetic pinning force, F_{mp} exists because of the magnetization gradient around the hole sites in the LSMO film. As it is schematically presented in Figure 10, $F_{mp} \propto -\nabla M_z$ is present at the LSMO grain edges, even when the magnetization is saturated perpendicularly. Also shown in Figure 10 is a three dimensional image of the LSMO surface, which, in the case of magnetic saturation, may correspond to the magnetic vortex pinning potential, U_{mp}. It can be seen that the anti-dots in the magnetic film act as potential wells where the vortices will be trapped. Because of the relatively high Curie temperature of the LSMO thin films[25] ~300 K, with respect to the investigated temperature range, 10–70 K, the magnetic pinning force, F_{mp} can be considered as temperature independent. On the other hand, the core pinning energy, $U_{cp} \propto (\Phi_0/8\pi\lambda_L)^2$, decreases as the temperature reaches T_c because of the increase in the London penetration length, $\lambda_L^{-2} \propto (T_c - T)$. Close to the critical

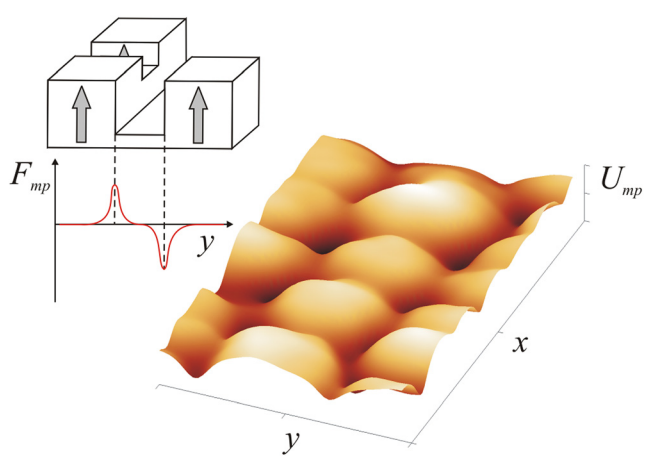

FIG. 10. Schematic presentation of the origin of F_{mp}, three-dimensional AFM image of the LSMO buffer layer surface, which, at saturation, may correspond to that of the magnetic vortex pinning potential, U_{mp}, within the YBCO film deposited on top.

temperature, T_c, F_{mp}, becomes greater than F_{cp}, which is zero at T_c, so that the magnetic pinning mechanism becomes dominant. From the $J_c(T)$ dependence presented in Figure 9, a cross-over temperature of 65 K may be observed, for which J_c becomes higher in the case of the YBCO/LSMO structure. This value of the cross-over temperature is in good agreement with the temperature dependence of the scaling law parameter, p, which shows that the proposed magnetic pinning mechanism becomes dominant at temperatures higher than 50 K.

IV. CONCLUSION

In the present paper, we have investigated the pinning properties of a nanostructured LSMO buffer layer on a YBCO thin film. The LSMO nanostructures were formed by the intrinsic film growth mode on a terraced STO (001) substrate and consisted of regular arrays of holes within the film, aligned along the substrate steps. Two contributions to the overall pinning mechanism were observed. One corresponds to the normal core pinning mechanism, while for the second pinning, a magnetic interaction between the magnetic flux of the vortices within the superconductor and the magnetization of the LSMO film is proposed. The magnetic pinning force is thought to arise due to the strong magnetization gradient present at the hole sites within the LSMO film, when it is perpendicularly saturated. The additional pinning contribution thus gives rise to an improved pinning strength at high fields and high temperatures, where condensation energy pinning becomes ineffective. Our assumptions demonstrate the necessity of a topographic modulation of magnetic films in order to obtain effective magnetic pinning in external magnetic fields above the saturation values, H_s.

ACKNOWLEDGMENTS

The authors acknowledge B. S. Vasile for the TEM analysis. This work has been partially supported by CNCSIS UEFISCSU, Project No. PNII IDEI No. 4/2010, code ID-106 and by POS CCE ID. 574, code SMIS-CSNR 12467.

[1]S. R. Foltyn, L. Civale, J. L. MacManus-Driscoll, Q. X. Jia, B. Maiorov, H. Wang, and M. Maly, Nature Mater. **6**, 631 (2007).
[2]L. N. Bulaevskii, E. M. Chudnovsky, and M. P. Maley, Appl. Phys. Lett. **76**, 2594 (2000).
[3]M. Velez, J. I. Martin, J. E. Villegas, A. Hoffmann, E. M. Gonzalez, J. L. Vicent, and I. K. Schuller, J. Magn. Magn. Mater. **320**, 2547 (2008).
[4]A. Yu Aladyshkin, A. V. Silhanek, W. Gillijns, and V. V. Moshchalkov, Supercond. Sci. Technol. **22**, 053001 (2009).
[5]S. C. Wimbush, J. H. Durrell, C. F. Tsai, H. Wang, Q. X. Jia, M. G. Blamire, and J. L. MacManus-Driscoll, Supercond. Sci. Technol. **23**, 045019 (2010).
[6]J. Albrecht, S. Soltan, and H.-U. Habermeier, Phys. Rev. B **72**, 092502 (2005).
[7]C. Z. Chen, C. B. Cai, L. Peng, B. Gao, F. Fan, Z. Y. Liu, Y. M. Lu, R. Zeng, and S. X. Dou, J. Appl. Phys. **106**, 093902 (2009).
[8]C. Z. Chen, Z. Y. Liu, Y. M. Lu, L. Zeng, C. B. Cai, R. Zeng, and S. X. Dou, J. Appl. Phys. **109**, 073921 (2011).
[9]A. K. Jha, N. Khare, and R. Pinto, J. Appl. Phys. **110**, 113920 (2011).
[10]V. Pena, Z. Sefrioui, D. Arias, C. Leon, J. Snatamaria, J. L. Martinez, S. G. E. de Velthuis, and A. Hoffmann, Phys. Rev. Lett. **94**, 057002 (2005).
[11]N. M. Nemes, C. Visani, Z. Sefrioui, C. Leon, J. Santamaria, M. Iglesias, F. Mompean, and M. García-Hernández, Phys. Rev. B **81**, 024512 (2010).
[12]Y. Liu, C. Visani, N. M. Nemes, M. R. Fitzsimmons, L. Y. Zhu, J. Tornos, M. García-Hernández, M. Zhernenkov, A. Hoffmann, C. Leon, J. Santamaria, and S. G. E. de Velthuis, Phys. Rev. Lett. **108**, 207205 (2012).
[13]H. Lüth, *Solid Surfaces, Interfaces and Thin Films* (Springer, 2001).
[14]S. Proyer, E. Stangl, M. Borz, B. Hallebrand, and D. Bäuerle, Physica C **257**, 1 (1996).
[15]T. Aytug, M. Paranthaman, B. W. Kang, S. Sathyamurthy, A. Goyal, and D. K. Christen, Appl. Phys. Lett. **79**, 2205 (2001).
[16]A. Boulle, R. Guinebretière, and A. Dauger, J. Phys. D: Appl. Phys. **38**, 3907 (2005).
[17]A. Boulle, R. Guinebretière, and A. Dauger, J. Appl. Phys. **97**, 073503 (2005).
[18]E. M. Gyorgy, R. B. van Dover, K. A. Jackson, L. F. Schneemeyer, and J. V. Waszczak, Appl. Phys. Lett. **55**, 283 (1989).
[19]X. Song, Z. Chen, S. I. Kim, D. M. Feldmann, D. Larbalestier, J. Reeves, Y. Xie, and V. Selvamanickam, Appl. Phys. Lett. **88**, 212508 (2006).
[20]S. Oh, H. Choi, C. Lee, H. Yamada, and H. Yamasaki, J. Appl. Phys. **102**, 043904 (2007).
[21]S. Senoussi, M. Oussena, G. Collin, and I. A. Campbell, Phys. Rev. B **37**, 9792 (1988).
[22]M. Sparing, E. Backen, T. Reudenberg, R. Hühne, B. Rellinghaus, L. Schultz, and B. Holzapfel, Supercond. Sci. Technol. **20**, S239 (2007).
[23]M. Mathews, F. M. Postma, J. Cock Lodder, R. Jansen, G. Rijnders, and D. H. A. Blanka, Appl. Phys. Lett. **87**, 242507 (2005).
[24]J. Dho, Y. N. Kim, Y. S. Hwang, J. C. Kim, and N. H. Hur, Appl. Phys. Lett. **82**, 1434 (2003).
[25]T. Petrisor, Jr., M. S. Gabor, A. Boulle, C. Bellouard, C. Tiusan, O. Pana, and T. Petrisor, J. Appl. Phys. **109**, 123913 (2011).
[26]L. Ranno, A. Llobet, R. Tiron, and E. Favre-Nicolin, Appl. Surf. Sci. **188**, 170 (2002).